

METAL ABUNDANCES OF RED CLUMP STARS IN OPEN CLUSTERS: I. NGC 6819 ¹

Angela Bragaglia¹, Eugenio Carretta², Raffaele G. Gratton², Monica Tosi¹, Giovanni Bonanno³, Pietro Bruno³, Antonio Cali³, Riccardo Claudi², Rosario Cosentino³, Silvano Desidera⁴, Giancarlo Farisato², Mauro Rebeschini², Salvo Scuderi³

¹Osservatorio Astronomico di Bologna, via Ranzani 1, 40127 Bologna, Italy

angela@bo.astro.it, tosi@bo.astro.it

²Osservatorio Astronomico di Padova, vicolo Osservatorio 5, 35122 Padova, Italy

carretta, gratton, claudi, farisato, rebeschini @pd.astro.it

³Osservatorio Astrofisico di Catania, Via S. Sofia 78, 95125, Catania, Italy

gbo@sunct.ct.astro.it

⁴Dipartimento di Astronomia, Università di Padova, Vicolo Osservatorio 5, 35122 Padova,
Italy

desidera@pd.astro.it

Received _____; accepted _____

ABSTRACT

We present an analysis of high dispersion spectra ($R \sim 40,000$) of three red clump stars in the old open cluster NGC 6819. The spectra were obtained with SARG, the high dispersion spectrograph of the Telescopio Nazionale Galileo. The spectra were analyzed using both equivalent widths measured with an automatic procedure, and comparisons with synthetic spectra. NGC 6819 is found to be slightly metal-rich ($[\text{Fe}/\text{H}] = +0.09 \pm 0.03$, internal error); there are no previous high resolution studies to compare with. Most element-to-element abundance ratios are close to solar; we find a slight excess of Si, and a significant Na overabundance. Our spectra can also be used to derive the interstellar reddening towards the cluster, by comparing the observed colours with those expected from line excitation: we derive $E(B - V) = 0.14 \pm 0.04$, in agreement with the most recent estimate for this cluster.

Subject headings: open clusters and associations: individual (NGC 6819) – stars: basic parameters – stars: stellar models – stars: abundances – techniques: spectroscopic

¹Based on observations made with the Italian Telescopio Nazionale Galileo (TNG) operated on the island of La Palma by the Centro Galileo Galilei of the CNAA (Consorzio Nazionale per l’Astronomia e l’Astrofisica) at the Spanish Observatorio del Roque de los Muchachos of the Instituto de Astrofísica de Canarias

1. INTRODUCTION

Open clusters (OC's) are excellent tools to infer the evolution of our Galaxy from both the chemical and structural points of view, because they provide information on the distribution of the chemical abundances in the disk, on the average ages at various galactic locations, on the initial mass function, on the interactions between thin and thick disks (e.g., Mayor 1976, Panagia and Tosi 1981, Friel 1995, Luhman et al. 2000). The major advantage of using OC's rather than field stars to derive these quantities resides in the circumstance that a) their current galactic location is not too different from where they were born, and b) the distances, ages and metallicities of field stars located beyond a limited radius from the sun are highly uncertain.

OC's probably represent the best means to understand how element abundances change with time and with location in the Galaxy. Several years ago, young OC's have been suggested to show steeper negative abundance gradients with galactocentric distance than old clusters (Mayor 1976, Panagia & Tosi 1981). However, later extensive studies (e.g. Friel & Janes 1993) have suggested that the gradient slope is roughly independent of the cluster age. A striking characteristic of Friel & Janes' sample is that at each Galactic radius the oldest clusters happen to be also the most metal rich ones. This result, if confirmed, would have remarkable implications on our understanding of the Galaxy evolution, since it is opposite to any intuitive age-metallicity relation derivable from steady-state scenarios and suggests the existence of short, intense phenomena which may alter significantly local evolutions. A caveat on these results is that they can be strongly affected by several uncertainties related also to the lack of homogeneity in the derivation of the cluster parameters (age, metallicity, distance, reddening). As discussed e.g. by Bragaglia et al. (2000), use of literature values can lead to a confusing picture; for instance, ages derived with different techniques/isochrones may not only be uncertain in absolute value, but also in ranking.

To overcome this problem, we are homogeneously analysing with great accuracy a sample of open clusters at various galactic locations and covering a wide range in age and metallicity. We derive the age, distance, reddening and approximate metallicity of these systems from deep photometry combined with the synthetic Color-Magnitude diagrams method (see e.g. Sandrelli et al. 1999 and references therein), while accurate element abundance determination is based on high-resolution spectroscopy. The final sample of OC's necessary to allow for significant statistics on the abundance gradient at various epochs should be of at least 30 objects.

In this paper we present the abundances derived from high-resolution spectroscopy of the first cluster of the sample: NGC 6819, an intermediate age cluster (age $\simeq 2.3$ – 3.1 Gyr), with RA(2000) = 19 41, DEC(2000) = +40 12, $l_{\text{II}} = 73.98^\circ$, $b_{\text{II}} = 8.47^\circ$, and Galactocentric distance 8.2 kpc. A recent reference for photometry and derivation of distance and age is Rosvick & VandenBerg (1998).

The observations have been performed with SARG, the new high dispersion spectrograph at the Italian Telescopio Nazionale Galileo (TNG) and this is the first paper where data acquired with this instrument are presented.

2. OBSERVATIONS AND DATA REDUCTION

Spectra of two clump stars were obtained in July 2000, and one in August 2000, during the second and third commissioning runs of SARG, the new high dispersion spectrograph at the 3.5 m TNG in La Palma (Spain). The stars were selected (using BDA, the database for Galactic open clusters, Mermilliod 1995) among fiducial cluster members, selected from proper motions (Sanders 1972), and now confirmed by the velocities measured from our spectra. The most important data for the program stars are listed in Table 1, along with

a summary of the spectral characteristics, and the heliocentric radial velocities; Figure 1 gives the location of the stars in the colour magnitude diagram (top panel) and on the sky (bottom panel).

Being this the first paper based on SARG data, a few details about the spectrograph and the observations are to be provided. SARG (Gratton et al. 2000, in preparation) is a single-arm, white-pupil, cross dispersed echelle spectrograph, permanently mounted at one of the arms of the TNG fork. It is fed by a suitable optical train from the Nasmyth focus. The spectrograph uses an R4 echelle grating in an off-plane, quasi-Littrow configuration, that yields an RS product of 46,000 when coupled with the 100 mm spectrograph beam. Spectral resolution of SARG depends on the selected slit (a set of 7 is available on the slit wheel, from 0.27 to 1.60 arcsec), the maximum value being about 150,000. The present observations were obtained using a slit width of 300 μm , corresponding to 1.60 arcsec projected on the sky. However, stellar images did not fill completely this wide slit. During the observations, the seeing value was about 0.7 arcsec. Since the guiding accuracy was not yet optimal (only manual guiding was available when the program spectra were acquired), the actual images over the 1 hr exposure time had a FWHM of about 1.2 arcsec, yielding a spectral resolution of about 40,000. This value is confirmed by measures of the FWHM of narrow telluric lines.

SARG is equipped with four grism cross dispersers mounted on a wheel; the present observations were done using the *yellow* grism, which provides an almost complete spectral coverage from 4650 to 7900 \AA , with only a small gap of about 40 \AA near 6200 \AA , due to the non-sensitive region between the two $4k \times 2k$ thinned, back illuminated EEV CCD's located on the focal plane of the spectrograph. Minimum interorder separation is about 7 arcsec. To reduce read out noise and read out time, the CCD's were binned 4×4 . With this choice, 2-pixel resolution is 36,000, a bit less than the FWHM of the spectral lines, so that the spectra are slightly undersampled. The spectra have a rather high background level, due to

parasite light in the spectrograph not yet eliminated when they were acquired, which is well removed by the spectrum extraction procedure. The high background level has small impact on the spectra of these rather bright stars and the final $S/N \sim 130$ is that expected from photon noise.

Spectral extraction was done using standard IRAF² routines for echelle spectra. First, the two CCD's were separated and reduced independently. The two dimensional images were bias subtracted (but not flat-fielded; the flats were extracted and used to check the quality of correction done for the blaze function, with the ISA package, Gratton 1988), then cleaned from cosmic rays hits and hot pixels using *cosmicrays*. Images were corrected for scattered light; the orders were then found (21 in the red CCD, and 34 in the blue one), traced, and extracted, subtracting the local sky background. Wavelength calibration was performed using thorium lamp exposures taken once each night (the spectrograph is very stable, and furthermore precise radial velocities were not our goal), yielding a *r.m.s* of about 0.009 Å in our wavelengths.

3. ANALYSIS AND ERROR ESTIMATES

3.1. Equivalent Widths

In our analysis, we used both equivalent widths and spectral synthesis. Equivalent widths were used to derive the best set of atmospheric parameters (effective temperature from line excitation, gravity from the equilibrium of ionization, microturbulence from trends with expected line strength: see Table 2) and elemental abundances. Comparisons with synthetic spectra were then used to check the adopted abundances.

²IRAF is distributed by the NOAO, which are operated by AURA, under contract with NSF

Equivalent widths (see Table 3) were measured on the unidimensional, extracted spectral orders using an automatic routine within the ISA package, prepared by one of us (R.G.G.). Only the spectral region 5500-7200 Å was eventually used in the abundance analysis: continuum tracing is quite uncertain at shorter wavelengths at the resolution of our spectra, and diffraction fringes (not completely removed by our reduction procedure) make results from longer wavelengths uncertain. The routine measuring equivalent widths works as follows. First, removal of the blaze function response is performed using a spline interpolating function. Then, a local continuum level is determined for each line by an iterative clipping average over a fraction (the highest ones) of the 200 spectral points centered on the line to be measured; after various tests, this fraction was set at 1/4th for the spectra of NGC 6819. Second, the equivalent width for each line from an extensive list (including several hundred lines, that are quite clean in the solar spectrum) is tentatively measured using a gaussian fitting routine. Measures are rejected according to several criteria (e.g. if the central wavelength does not agree with that expected from preliminary measure of the geocentric radial velocity; if the lines are too broad or too narrow, etc.). Third, the measured lines are used to draw a relationship between equivalent width and FWHM. Fourth, this relation is used to measure again equivalent widths using a second gaussian fitting routine, which has only one free parameter (the equivalent width), since the central wavelength is fixed by the measured geocentric radial velocity, and the FWHM by the relationship between equivalent width and FWHM. Again measures are rejected if residuals are too large, asymmetric, etc.

These procedures allow one to obtain very stable measures of the EWs, with small random errors even when lines are in quite crowded spectral regions. However, systematic errors may be present, related to the adopted reference continua. Comparisons with synthetic spectra convinced us that systematic errors in the finally adopted EWs are quite small, insofar as a suitable fraction of the points is used to determine the reference continuum level and rejection criteria on the used lines are kept strict.

Since the stars have similar atmospheric parameters, we may estimate (internal) errors in our equivalent widths by comparing values measured in different stars. Such a comparison is shown in Figure 2. Taking as reference star 978 (which is the brightest, and has the best spectrum), the *rms* scatter about the linear relationship are 10.9 and 10.5 mÅ for stars 333 and 979 respectively. Assuming that both sets of EWs have equal errors, we can estimate typical errors of 7.5 mÅ in our measured EWs.

3.2. Atmospheric parameters

Equivalent widths and Kurucz model atmospheres (CD-ROM 13: models with the over-shooting option switched off) were used to derive the best set of atmospheric parameters listed in Table 2. Effective temperatures were derived directly from the spectra, imposing Fe I lines of different excitation (several tens for each star) to provide the same temperatures. Panel (a) of Figure 3 shows the run of abundances from Fe I lines with excitation potential for star 978: there is no discernible trend. Internal error estimates in temperatures are obtained directly from the errors in the linear regression fits, and are ± 68 K, corresponding to 1σ *rms* uncertainty of 0.015 dex/eV in the slope. Systematic errors might be larger and mainly ascribed to the set of adopted model atmospheres (Kurucz 1995).

In addition, a number of Fe II lines were measured in each star, allowing to estimate surface gravities $\log g$ from the equilibrium of ionization of Fe, which is very well derived from our Fe lines. Internal errors include contribution from both the above uncertainties in the adopted temperature and the errors in EWs of individual lines: the quadratic sums provide an internal error of ± 0.19 dex in $\log g$. Our use of the LTE approximation in the analysis is not of concern for these stars (see Gratton et al. 1999); however, systematic errors can be present, mainly related again to the adopted model atmospheres.

The following exercise shows that the assumed temperature scale leads to a reasonable internal consistency of data. The (average) absolute magnitude of the program stars is $M_V = +0.6$, according to their apparent magnitude and to the distance modulus of $(m - M)_V = 12.35$ by Rosvick & Vandenberg (1998), and in agreement with the average value for clump stars measured by Hipparcos. The bolometric correction appropriate for the temperature, gravity and metal abundances of the program stars, derived from the Kurucz CD-ROM's is $BC = -0.44$ mag. This leads to an assumed luminosity of the program stars of $\log L/L_\odot = 1.82$, and, assuming a mass of 1.5–1.6 M_\odot (appropriate for a clump star in a 2.5 Gyr old cluster: see Rosvick & Vandenberg 1998), we obtain an expected gravity for the program stars of $\log g = 2.5$, in reasonable agreement with the observed value. Note that, instead, if we decrease T_{eff} by 100 K, we obtain a good ionization equilibrium for a gravity of $\log g \sim 2.3$, that implies an absolute magnitude of $M_V \sim +0.3$: too bright in our opinion for clump stars in an old open cluster. This exercise thus suggests that the adopted temperature scale might be overestimated but only slightly (by $\simeq 50$ K); such a small error would cause our [Fe/H] value to be overestimated by only 0.03 dex. Hereinafter, we will assume that systematic errors are not larger than the internal errors of ± 70 K.

Microturbulent velocities v_t were obtained by compensating any trend in the derived abundances from Fe I lines with the expected line strength (see Magain 1984). Results for star 978 are graphically shown in panel (b) of Figure 3. Due to the large number of measured Fe I lines and to the high quality of measurements, internal error bars in the derived values of v_t are almost negligible (± 0.07 km/s, average from the 3 stars).

3.3. Abundances

Table 4 lists the abundances obtained for the individual stars, as well as the average values for the cluster. Sensitivities of these abundances to changes in the atmospheric param-

eters are listed in Table 5 and were used to estimate the internal errors in our abundances. These errors are given in the last column of Table 4 and were obtained by summing quadratically the contribution due to each atmospheric parameter (assuming uncertainties of 70 K in T_{eff} , 0.19 dex in $\log g$, 0.05 dex in $[A/H]$, and 0.07 km/s in v_t : last Column of Table 5), and that due to the line-to-line scatter (we assumed 0.15 dex); the value was then divided by the square root of the number of stars used to estimate abundances.

The average Fe abundance for NGC 6819 is $[\text{Fe}/\text{H}] = +0.09 \pm 0.03$, the three stars yielding very similar results. Element-to-element abundance ratios are generally close to solar (within twice the internal error; note that abundances for V, Mn, and Co include corrections for the quite large hyperfine structure of their lines). There are two exceptions:

- We get a slight overabundance of Si (on average, $[\text{Si}/\text{Fe}] = +0.18 \pm 0.04$). This result is obtained from a rather large number of lines and seems reasonably sound;
- We find a quite large Na excess (on average, $[\text{Na}/\text{Fe}] = +0.47 \pm 0.07$). This value includes a small non-LTE correction (< 0.05 dex), computed according to Gratton et al. (1999). A partial confirmation of the results of the equivalent width based abundance analysis comes from comparisons of the observed spectra with synthetic spectra. An example of such a comparison is shown in Figure 4, where the spectral region 6150-6166 Å is presented, compared with results of spectral synthesis computations. Note the good match of the Fe I lines. Na and Si lines are clearly stronger than predicted for a solar-scaled composition, indicating an overabundance with respect to Fe. However, the excess we would derive from this figure is about $[\text{Na}/\text{Fe}] \sim +0.3$, a bit lower than that given by the equivalent widths. Similar excesses of Na have been found for population I supergiants (see e.g. Sasselov 1986); however the clump stars in NGC 6819 are much less massive than those considered by Sasselov.

4. SUMMARY AND CONCLUSIONS

We can use our temperatures, derived from line excitation (and hence a reddening free parameter) to derive the interstellar reddening toward NGC 6819. This can be done by comparing the observed ($B-V$) colours with those predicted by models (Kurucz 1995). There might be some systematic errors in such reddening derivations, since they would depend on the accuracy of the colours computed by model atmospheres, and on possible errors on the gf 's. However, this zero-point offset (itself a function of temperature) may be determined by observation of a comparison sample of nearby, unreddened clump stars, analyzed following strictly the same procedure described here. We did this for a sample of 12 bright clump stars with accurate parallaxes from Hipparcos (Cohen et al. 2000, in preparation). This comparison sample overlaps in temperature and metal abundance the stars of NGC 6819, so that no extrapolation was required. Using this procedure, we derive an average reddening for our three clump stars of $E(B - V) = 0.142 \pm 0.044$ (3 stars, r.m.s.=0.076 mag). This value agrees very well with that obtained recently by Rosvick & Vandenberg ($E(B - V) = 0.16$) in their accurate study based on good quality CCD photometry. Previous determinations were contradictory, ranging e.g. from $E(B - V) = 0.12$ (Burkhead 1971) to $E(B - V) = 0.28$ (Auner 1974), and were based on more uncertain photographic photometry.

Our determination of the metallicity for NGC 6819 ($[\text{Fe}/\text{H}] = +0.09 \pm 0.03$) is only slightly higher than the value obtained by Rosvick & Vandenberg (1998) from an analysis of the color-magnitude diagram ($[\text{Fe}/\text{H}] = -0.05$), and seems to agree very well with the value given by Twarog, Ashman & Anthony-Twarog (1997: $[\text{Fe}/\text{H}] = +0.07 \pm 0.05$), and based on a revision of the low dispersion spectroscopic data by Friel & Janes (1993). In fact the latter agreement is based on a value for the reddening ($E(B - V) = 0.28 - 0.30$) much higher than ours, derived from quite old data and explicitly admitted to be highly uncertain. Had they adopted a lower value for the reddening, their metallicity would have also been lower ($[\text{Fe}/\text{H}]$

$\simeq -0.05$ or -0.10 , see Rosvick & Vandenberg 1998), but the discrepancy is fairly modest.

Our values for the metallicity and reddening of NGC6819 are close enough to the values presented by Rosvick & Vandenberg that no new analysis of distance modulus and age for this cluster seems required. We must recall, however, that the age and distances derived from isochrone fitting to the cluster color-magnitude diagram are highly sensitive to the adopted stellar models. Finally, we point out that our reddening and metallicity perfectly agree with those recently adopted by Sarajedini (1999) in his discussion of the dependence of the luminosity of the clump on age and metallicity.

NGC6819 hence appears to be a cluster with galactocentric distance (8–9 kpc) similar to that of the sun, metallicity moderately higher and age slightly younger. These features make it consistent with standard age-metallicity relations and abundance gradients.

We acknowledge the use of the BDA, the open clusters database maintained by J.C. Mermilliod. This research has made use of the SIMBAD data base, operated at CDS, Strasbourg, France. We thank the referee for thorough comments and useful suggestions. Financial support has been provided by the Italian MURST, through COFIN-1998 under the project "Stellar Evolution". Partial support by CNAA is also acknowledged.

REFERENCES

- Auner, G. 1974, *A&A*, 13, 143
- Bragaglia, A., Tosi, M., Marconi, G., & Carretta, E. 2000, in *The Evolution of the Milky Way. Stars vs Clusters*, F.Giovanelli, F.Matteucci eds (Kluwer, Dordrecht), in press (astro-ph/9912130)
- Burkhead, M.S. 1971, *AJ*, 76, 251
- Friel, E.D. 1995, *ARA&A*, 33, 38
- Friel, E.D., & Janes, K.A. 1993, *A&A*, 267, 75
- Gratton, R.G. 1988, Rome Obs. Preprint Ser. 29
- Gratton, R.G., Carretta, E., Gustafsson, B., & Eriksson, K. 1999, *A&A*, 350, 955
- Kurucz, R.L. 1995, CD-ROM 13
- Luhman, K.L., Rieke, G.H., Young, E.T., Cotera, A.S., Chen, H., Rieke, M.J., Schneider, G., & Thompson, R.I. 2000, *ApJ*, in press (astro-ph/0004386)
- Magain, P. 1984, *A&A*, 134, 189
- Mayor, M. 1976, *A&A*, 48, 301
- Mermilliod, J.C. 1995, D. Egret, M.A. Albrecht eds, *Information and On-Line Data in Astronomy*, Kluwer Academic Press (Dordrecht), p. 127
- Panagia, N., & Tosi, M. 1981, *A&A*, 96, 306
- Rosvick, J.M., & Vandenberg, D.A. 1998, *AJ*, 115, 1516
- Sanders, W.L. 1972, *A&A*, 19, 155
- Sandrelli, S., Bragaglia, A., Tosi, M., & Marconi, G. 1999, *MNRAS*, 309, 739
- Sarajedini, A. 1999, *AJ*, 118, 2321

Sasselov, D.D. 1986, *PASP*, 98, 561

Twarog, B.A., Ashman, K., & Anthony-Twarog, B. 1997, *AJ*, 114, 2556

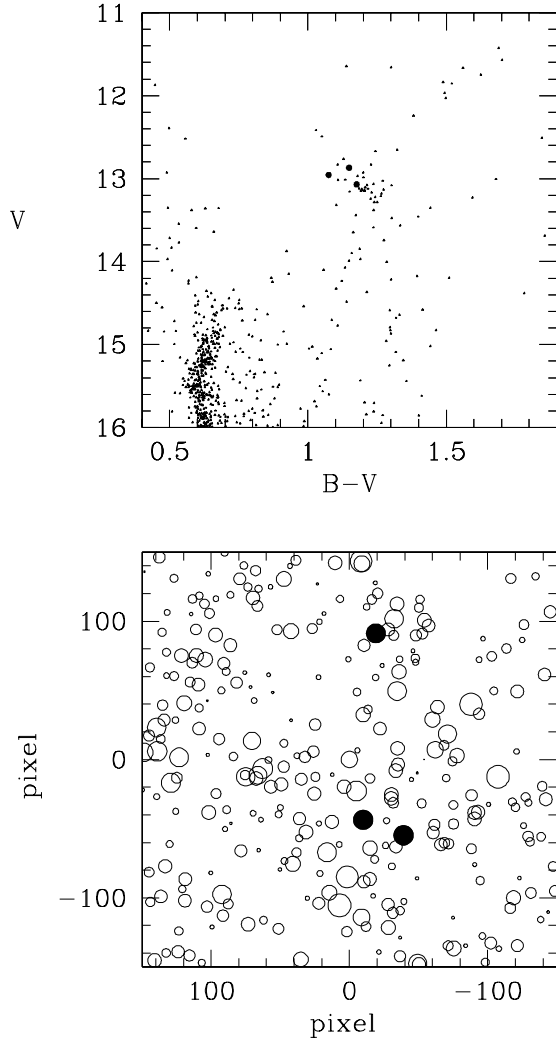


Fig. 1.— Top panel: CMD for NGC 6819, taken from Rosvick & Vandenberg (1998). The three observed stars are shown with a heavier mark. Bottom panel: cluster map (field of 2.8 arcmin², East on the left, North up) with the three observed clump stars plotted as filled circles: from top to bottom 333, 979, and 978.

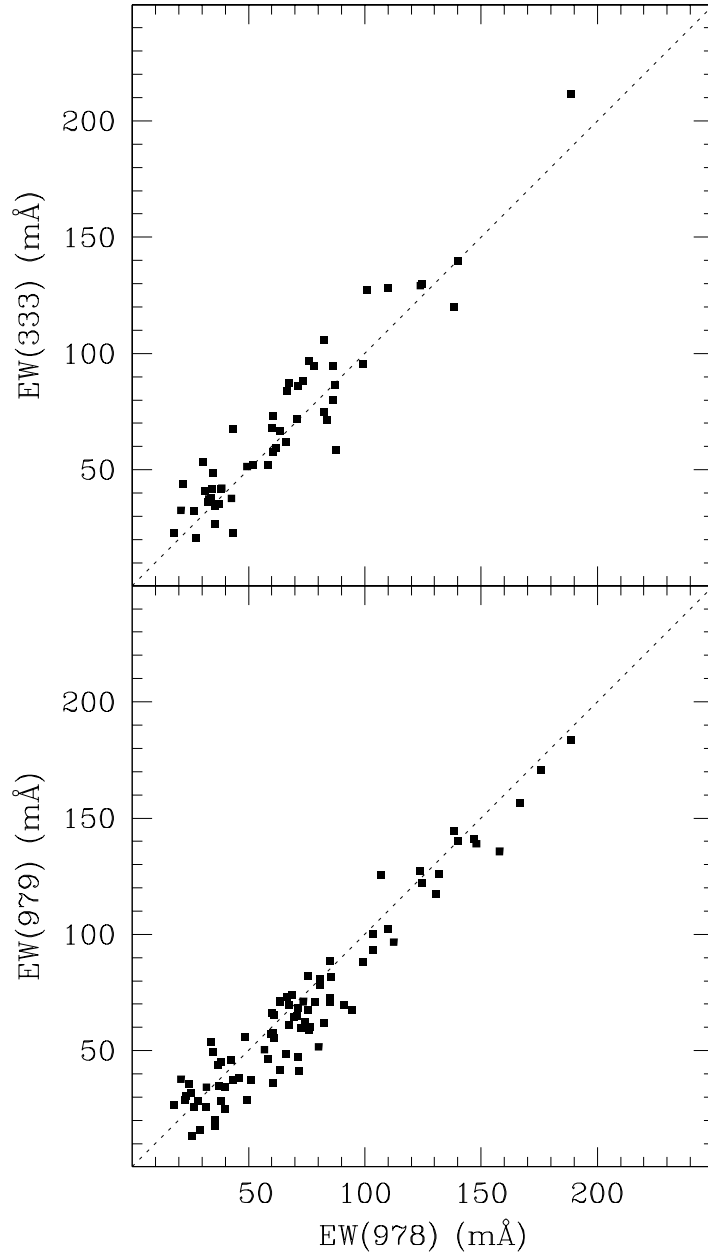


Fig. 2.— Comparisons between the equivalent widths measured in star 978, and those measured in star 333 (top panel) and 979 (bottom panel).

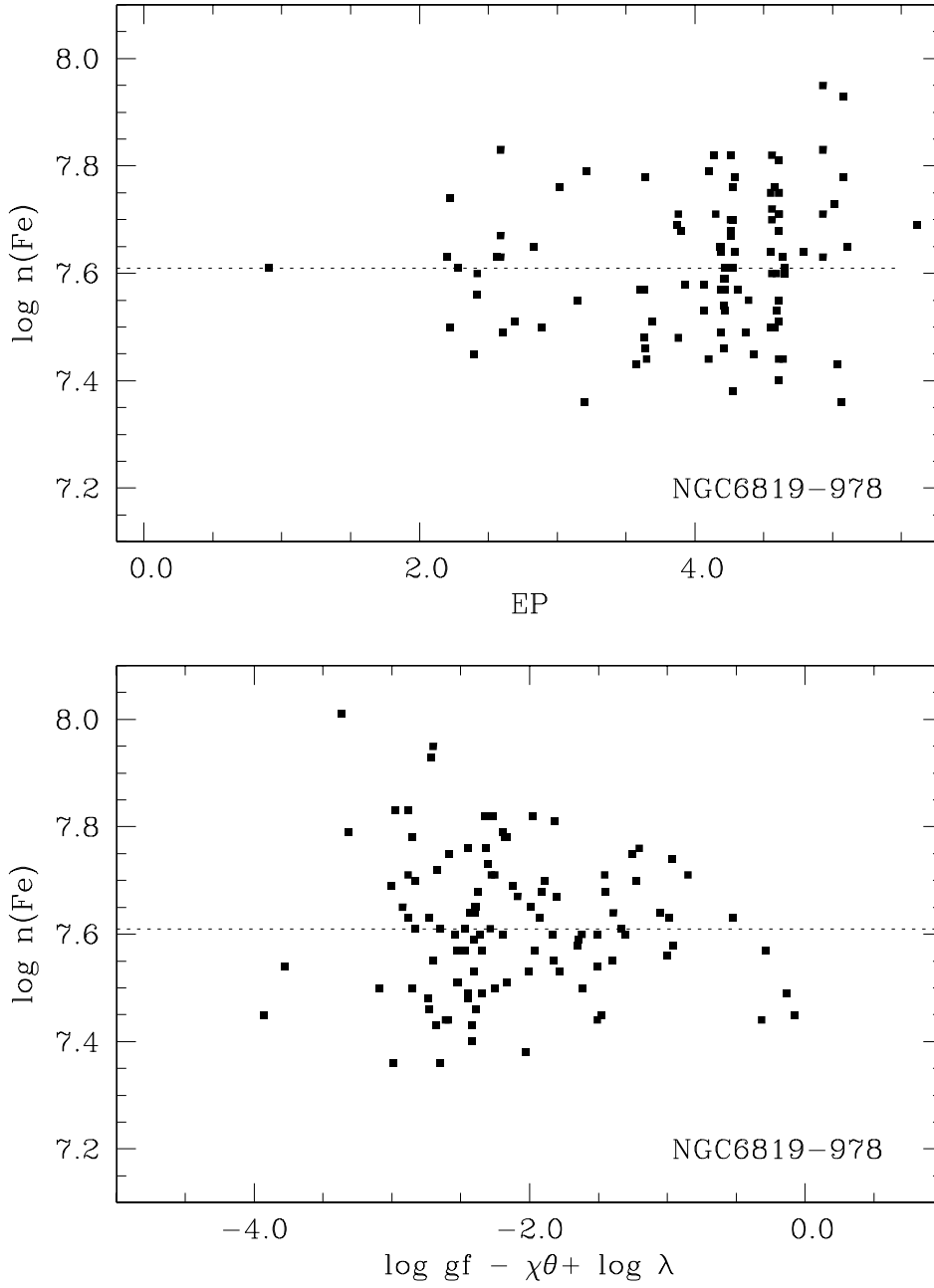


Fig. 3.— Trends of abundances from individual Fe I lines with excitation potential (top panel) and expected line strength (bottom panel) for star 978.

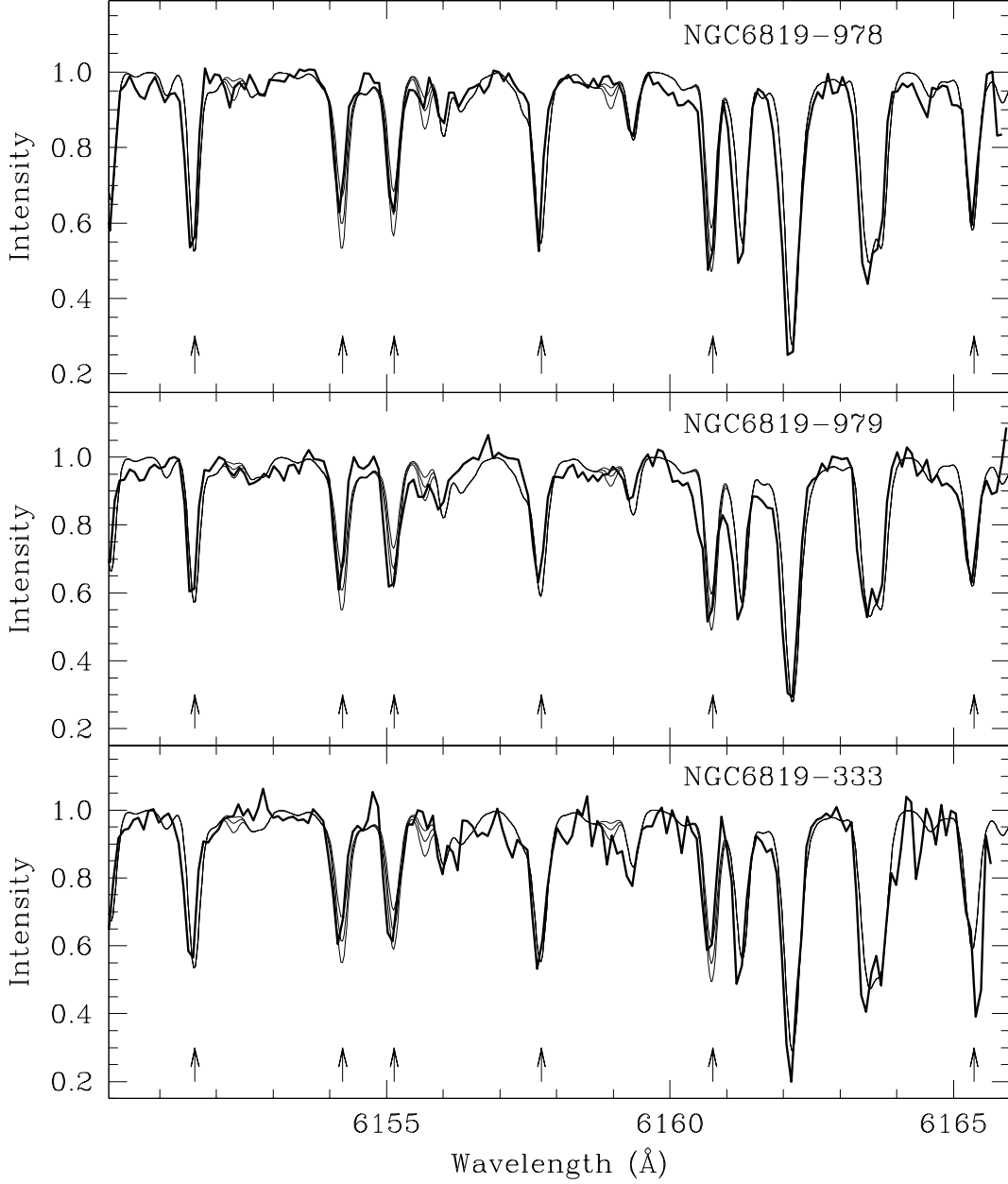


Fig. 4.— Spectra of the observed stars in the region 6150-6165 Å (thick lines), compared with synthetic spectra computed with the appropriate atmospheric parameters and abundances, and three different values of Na and Si abundances ($[\text{Na}/\text{Fe}] = 0.0, 0.3, \text{ and } 0.6$; $[\text{Si}/\text{Fe}] = 0.0, 0.3, \text{ and } 0.6$: thin lines). Lines of Na, Si and Fe are marked (Na I 6154.230 and 6160.753, Si I 6155.135, Fe I 6151.623, 6157.733, and 6165.363). Note the good match of the Fe I lines. Na and Si are clearly overabundant with respect to Fe.

Table 1: Information on the observed stars; the RV’s are heliocentric, and derived from about one hundred FeI lines in each spectrum. Identification is taken from the BDA (Mermilliod 1995: an extension of the Auner 1974 numeration), photometry from Rosvick & VandenBerg (1998), and membership from Sanders (1972)

Ident	RA (2000)	Dec (2000)	V	B–V	prob. memb.	Date obs	UT init.	exptime sec	RV kms ^{−1}
333	19 41 20	+40 12 41	13.069	1.176	92	2000/08/17	00:45:41	3600	5.31
978	19 41 15	+40 11 05	12.869	1.149	90	2000/07/18	01:14:35	3600	5.96
979	19 41 17	+40 11 11	12.956	1.075	91	2000/07/18	02:20:19	3600	1.44

Table 2: Adopted atmospheric parameters and iron abundances

star	T_{eff}	$\log g$	v_t	[Fe/H]
	(K)	(dex)	(km/s)	
333	4835	2.61	1.54	0.11
978	4855	2.60	1.26	0.11
979	4740	2.72	0.98	0.11

Table 3: Equivalent widths. The first column for each star is the equivalent width (in mÅ); the second one the abundance derived from this line ($\log n(A)$, in the scale where $\log n(H) = 12$)

Element	Wavel.	E.P.	log gf	333		978		979	
NaI	5688.22	2.10	-0.37	0.0	0.00	0.0	0.00	151.5	6.32
NaI	6154.23	2.10	-1.57	109.4	6.77	0.0	0.00	105.1	6.81
NaI	6160.75	2.10	-1.26	120.2	6.60	138.4	6.96	144.6	7.04
MgI	5528.42	4.34	-0.48	0.0	0.00	0.0	0.00	212.1	7.12
MgI	5711.09	4.34	-1.71	138.0	7.50	0.0	0.00	0.0	0.00
MgI	6318.71	5.11	-1.97	0.0	0.00	71.5	7.65	41.2	7.17
MgI	6319.24	5.11	-2.20	0.0	0.00	0.0	0.00	37.0	7.32
AlI	6696.03	3.14	-1.32	0.0	0.00	80.2	6.44	51.6	5.95
AlI	6698.67	3.14	-1.62	58.1	6.35	0.0	0.00	60.6	6.40
SiI	5645.62	4.93	-2.14	62.0	7.72	65.9	7.83	0.0	0.00
SiI	5665.56	4.92	-2.04	0.0	0.00	0.0	0.00	73.2	7.98
SiI	5684.49	4.95	-1.65	92.8	7.76	0.0	0.00	88.8	7.90
SiI	5690.43	4.93	-1.87	58.4	7.39	87.6	7.95	0.0	0.00
SiI	5701.11	4.93	-2.05	67.8	7.72	60.0	7.63	66.4	7.87
SiI	5772.15	5.08	-1.75	0.0	0.00	85.1	7.93	88.5	8.13
SiI	5793.08	4.93	-2.06	66.7	7.71	63.8	7.71	71.2	7.96
SiI	5797.87	4.95	-2.05	0.0	0.00	0.0	0.00	53.7	7.65
SiI	5948.55	5.08	-1.23	0.0	0.00	107.1	7.78	125.5	8.16
SiI	6125.03	5.61	-1.57	51.3	7.70	49.4	7.69	0.0	0.00
SiI	6145.02	5.61	-1.44	0.0	0.00	0.0	0.00	67.4	8.00
SiI	6848.57	5.86	-1.75	22.9	7.58	43.1	8.01	0.0	0.00
S I	6748.78	7.87	-0.44	0.0	0.00	14.8	7.45	0.0	0.00
S I	6757.20	7.87	-0.29	0.0	0.00	19.8	7.54	0.0	0.00
CaI	5867.57	2.93	-1.49	65.4	6.35	0.0	0.00	49.8	6.11
CaI	6439.08	2.52	0.39	211.4	5.97	188.5	5.91	183.7	5.79
CaI	6449.82	2.52	-0.50	173.1	6.50	0.0	0.00	0.0	0.00
CaI	6455.60	2.52	-1.29	118.9	6.51	0.0	0.00	0.0	0.00
CaI	6499.65	2.52	-0.82	0.0	0.00	0.0	0.00	117.9	6.21
CaI	6572.80	0.00	-4.32	0.0	0.00	124.4	6.69	0.0	0.00

Table 3: Equivalent widths (cont...)

Element	Wavel.	E.P.	log gf	333		978		979	
ScI	5671.83	1.45	0.56	0.0	0.00	68.2	3.21	0.0	0.00
ScII	5526.82	1.77	0.19	115.9	2.98	0.0	0.00	101.2	3.12
ScII	5640.99	1.50	-0.86	88.3	3.18	0.0	0.00	0.0	0.00
ScII	5657.88	1.51	-0.29	0.0	0.00	112.5	3.30	96.7	3.19
ScII	5684.20	1.51	-0.92	86.5	3.22	87.2	3.37	0.0	0.00
ScII	6245.62	1.51	-1.05	0.0	0.00	85.0	3.38	71.0	3.30
ScII	6279.74	1.50	-1.16	0.0	0.00	73.6	3.26	71.1	3.40
ScII	6604.60	1.36	-1.14	0.0	0.00	80.9	3.18	81.1	3.37
TiI	5490.16	1.46	-0.93	0.0	0.00	72.7	4.91	59.8	4.59
TiI	5503.90	2.58	-0.19	59.8	5.15	0.0	0.00	0.0	0.00
TiI	5662.16	2.32	-0.11	0.0	0.00	77.3	5.19	0.0	0.00
TiI	5689.48	2.30	-0.47	51.8	4.97	58.3	5.16	46.2	4.86
TiI	5978.55	1.87	-0.58	0.0	0.00	94.6	5.40	0.0	0.00
TiI	6091.18	2.27	-0.42	0.0	0.00	66.3	5.18	48.6	4.78
TiI	6126.22	1.07	-1.42	95.7	5.07	99.4	5.32	0.0	0.00
TiI	6554.24	1.44	-1.22	0.0	0.00	91.1	5.36	69.8	4.91
V I	5627.64	1.08	-0.37	113.0	4.21	0.0	0.00	0.0	0.00
V I	5670.86	1.08	-0.42	109.0	4.17	0.0	0.00	0.0	0.00
V I	5703.59	1.05	-0.21	118.6	4.08	0.0	0.00	0.0	0.00
V I	6081.45	1.05	-0.58	105.8	4.16	82.4	3.90	62.0	3.44
V I	6090.22	1.08	-0.06	121.7	3.97	0.0	0.00	105.3	3.91
V I	6243.11	0.30	-0.98	0.0	0.00	0.0	0.00	104.0	3.75
V I	6251.83	0.29	-1.34	0.0	0.00	102.4	4.06	0.0	0.00
CrI	5702.33	3.45	-0.68	0.0	0.00	0.0	0.00	47.3	5.65
CrI	5781.19	3.32	-0.88	0.0	0.00	48.6	5.77	56.1	5.89
CrI	5783.07	3.32	-0.40	79.9	5.75	0.0	0.00	0.0	0.00
CrI	5784.98	3.32	-0.38	59.5	5.38	61.7	5.52	0.0	0.00
CrI	5787.93	3.32	-0.08	0.0	0.00	0.0	0.00	74.0	5.48
CrI	6330.10	0.94	-2.87	0.0	0.00	85.2	5.51	72.8	5.24
CrI	6883.07	3.44	-0.42	84.6	5.91	0.0	0.00	66.4	5.71
MnI	6013.50	3.07	-0.25	139.6	5.44	139.9	5.65	140.2	5.70

Table 3: Equivalent widths (cont...)

Element	Wavel.	E.P.	log gf	333		978		979	
MnI	6016.65	3.07	-0.09	156.4	5.54	0.0	0.00	0.0	0.00
MnI	6021.80	3.08	0.03	173.5	5.65	0.0	0.00	0.0	0.00
FeI	5491.84	4.19	-2.24	0.0	0.00	38.8	7.64	0.0	0.00
FeI	5494.47	4.07	-1.96	0.0	0.00	54.4	7.53	0.0	0.00
FeI	5522.45	4.21	-1.47	0.0	0.00	74.2	7.59	62.5	7.43
FeI	5539.29	3.64	-2.59	0.0	0.00	0.0	0.00	66.9	7.99
FeI	5547.00	4.22	-1.85	0.0	0.00	0.0	0.00	70.1	8.00
FeI	5552.69	4.95	-1.69	0.0	0.00	0.0	0.00	12.4	7.24
FeI	5560.22	4.43	-1.10	88.1	7.60	73.2	7.45	0.0	0.00
FeI	5568.86	3.63	-2.82	41.8	7.57	34.4	7.48	0.0	0.00
FeI	5577.03	5.03	-1.49	0.0	0.00	21.3	7.43	0.0	0.00
FeI	5595.05	5.06	-1.69	0.0	0.00	12.3	7.36	0.0	0.00
FeI	5608.98	4.21	-2.22	53.4	7.85	30.4	7.46	0.0	0.00
FeI	5609.97	3.64	-3.09	0.0	0.00	21.0	7.46	0.0	0.00
FeI	5611.36	3.63	-2.84	41.9	7.60	38.1	7.57	45.4	7.73
FeI	5618.64	4.21	-1.34	94.7	7.72	78.2	7.54	0.0	0.00
FeI	5619.61	4.39	-1.49	0.0	0.00	61.1	7.55	65.4	7.72
FeI	5635.83	4.26	-1.59	0.0	0.00	69.6	7.67	0.0	0.00
FeI	5636.70	3.64	-2.53	0.0	0.00	63.6	7.78	41.7	7.35
FeI	5650.00	5.10	-0.80	0.0	0.00	0.0	0.00	54.0	7.56
FeI	5651.48	4.47	-1.79	49.8	7.65	0.0	0.00	28.4	7.28
FeI	5652.33	4.26	-1.77	0.0	0.00	67.7	7.82	61.0	7.75
FeI	5677.69	4.10	-2.55	32.5	7.67	21.0	7.44	37.8	7.83
FeI	5678.39	3.88	-2.88	0.0	0.00	19.5	7.48	0.0	0.00
FeI	5680.24	4.19	-2.20	37.7	7.52	34.0	7.49	53.6	7.93
FeI	5701.56	2.56	-2.16	0.0	0.00	0.0	0.00	125.9	7.56
FeI	5717.84	4.28	-0.98	0.0	0.00	103.6	7.76	93.3	7.67
FeI	5731.77	4.26	-1.10	102.8	7.67	0.0	0.00	80.6	7.50
FeI	5738.24	4.22	-2.24	34.3	7.52	35.7	7.59	20.4	7.23
FeI	5741.86	4.26	-1.69	84.0	7.91	66.7	7.70	73.2	7.93
FeI	5742.96	4.18	-2.26	0.0	0.00	39.9	7.65	24.7	7.32

Table 3: Equivalent widths (cont...)

Element	Wavel.	E.P.	log gf	333		978		979	
FeI	5752.04	4.55	-0.92	0.0	0.00	85.5	7.64	81.9	7.67
FeI	5759.26	4.65	-1.98	0.0	0.00	25.5	7.60	13.2	7.21
FeI	5760.36	3.64	-2.46	0.0	0.00	0.0	0.00	61.5	7.71
FeI	5778.46	2.59	-3.44	0.0	0.00	75.5	7.67	82.0	7.92
FeI	5784.67	3.40	-2.53	66.3	7.42	0.0	0.00	0.0	0.00
FeI	5793.92	4.22	-1.62	0.0	0.00	63.8	7.53	70.8	7.76
FeI	5806.73	4.61	-0.93	71.3	7.32	83.8	7.68	0.0	0.00
FeI	5811.91	4.14	-2.27	0.0	0.00	0.0	0.00	36.3	7.55
FeI	5814.81	4.28	-1.81	67.4	7.75	43.2	7.38	37.4	7.27
FeI	5835.11	4.26	-2.18	0.0	0.00	40.8	7.68	0.0	0.00
FeI	5837.70	4.29	-2.21	26.6	7.42	35.6	7.64	0.0	0.00
FeI	5849.69	3.69	-2.86	40.8	7.66	31.1	7.51	0.0	0.00
FeI	5852.23	4.55	-1.36	0.0	0.00	0.0	0.00	51.7	7.45
FeI	5855.09	4.61	-1.56	46.8	7.51	0.0	0.00	33.3	7.31
FeI	5856.10	4.29	-1.57	67.7	7.53	0.0	0.00	73.1	7.85
FeI	5858.78	4.22	-2.19	35.3	7.49	37.3	7.57	34.8	7.53
FeI	5859.60	4.55	-0.63	117.4	7.78	0.0	0.00	0.0	0.00
FeI	5861.11	4.28	-2.26	36.1	7.65	32.4	7.61	0.0	0.00
FeI	5862.37	4.55	-0.42	0.0	0.00	0.0	0.00	107.3	7.63
FeI	5879.49	4.61	-1.90	0.0	0.00	22.8	7.40	28.8	7.56
FeI	5880.02	4.56	-1.85	0.0	0.00	0.0	0.00	27.5	7.42
FeI	5881.28	4.61	-1.76	0.0	0.00	43.6	7.71	0.0	0.00
FeI	5902.48	4.59	-1.86	48.7	7.82	34.8	7.60	49.4	7.94
FeI	5905.68	4.65	-0.78	94.8	7.62	86.4	7.61	0.0	0.00
FeI	5927.80	4.65	-1.07	71.9	7.50	71.1	7.60	65.1	7.56
FeI	5929.68	4.55	-1.16	87.1	7.75	67.4	7.50	69.7	7.63
FeI	5930.19	4.65	-0.34	123.0	7.65	0.0	0.00	108.4	7.66
FeI	5933.80	4.64	-2.05	23.1	7.56	17.9	7.44	26.6	7.68
FeI	5934.66	3.93	-1.08	128.3	7.70	109.9	7.58	102.2	7.54
FeI	5947.53	4.61	-1.95	22.5	7.41	0.0	0.00	0.0	0.00
FeI	5969.57	4.28	-2.63	0.0	0.00	20.7	7.70	0.0	0.00

Table 3: Equivalent widths (cont...)

Element	Wavel.	E.P.	log gf	333		978		979	
FeI	5976.79	3.94	-1.30	0.0	0.00	0.0	0.00	103.9	7.81
FeI	5984.83	4.73	-0.29	119.3	7.63	0.0	0.00	112.0	7.74
FeI	6003.02	3.88	-1.02	129.1	7.60	124.0	7.71	127.4	7.85
FeI	6007.97	4.65	-0.76	80.0	7.34	86.5	7.60	0.0	0.00
FeI	6008.57	3.88	-0.92	120.4	7.35	0.0	0.00	116.7	7.59
FeI	6015.24	2.22	-4.57	0.0	0.00	31.6	7.50	25.9	7.33
FeI	6019.37	3.57	-3.14	43.7	7.84	21.8	7.43	0.0	0.00
FeI	6027.06	4.07	-1.20	96.8	7.42	0.0	0.00	0.0	0.00
FeI	6034.04	4.31	-2.30	20.9	7.38	27.3	7.57	0.0	0.00
FeI	6054.08	4.37	-2.17	32.1	7.57	26.5	7.49	25.9	7.47
FeI	6056.01	4.73	-0.46	116.0	7.75	0.0	0.00	109.0	7.86
FeI	6065.49	2.61	-1.49	0.0	0.00	175.9	7.49	170.7	7.44
FeI	6078.50	4.79	-0.38	127.2	7.90	100.8	7.64	0.0	0.00
FeI	6079.02	4.65	-0.97	96.7	7.85	76.2	7.60	59.1	7.33
FeI	6089.57	5.02	-0.87	73.4	7.75	0.0	0.00	60.5	7.67
FeI	6093.65	4.61	-1.32	85.8	7.95	71.4	7.81	47.3	7.38
FeI	6094.38	4.65	-1.56	0.0	0.00	0.0	0.00	42.8	7.56
FeI	6096.67	3.98	-1.76	75.8	7.48	0.0	0.00	69.5	7.58
FeI	6098.25	4.56	-1.81	0.0	0.00	49.6	7.82	0.0	0.00
FeI	6120.26	0.91	-5.77	0.0	0.00	59.8	7.61	57.1	7.53
FeI	6137.00	2.20	-2.91	133.5	7.54	0.0	0.00	0.0	0.00
FeI	6151.62	2.18	-3.26	124.6	7.70	0.0	0.00	97.4	7.51
FeI	6157.73	4.07	-1.26	0.0	0.00	0.0	0.00	95.3	7.72
FeI	6246.33	3.60	-0.73	0.0	0.00	158.0	7.57	135.7	7.34
FeI	6252.56	2.40	-1.64	0.0	0.00	183.5	7.45	0.0	0.00
FeI	6270.23	2.86	-2.55	0.0	0.00	0.0	0.00	106.0	7.84
FeI	6290.55	2.59	-4.27	37.6	7.70	42.6	7.83	46.0	7.88
FeI	6297.80	2.22	-2.70	0.0	0.00	142.2	7.74	0.0	0.00
FeI	6301.51	3.65	-0.72	0.0	0.00	146.9	7.44	140.9	7.42
FeI	6311.50	2.83	-3.16	0.0	0.00	78.4	7.65	71.1	7.59
FeI	6315.81	4.07	-1.67	0.0	0.00	75.6	7.58	67.5	7.51

Table 3: Equivalent widths (cont...)

Element	Wavel.	E.P.	log gf	333		978		979	
FeI	6322.69	2.59	-2.38	0.0	0.00	130.7	7.63	117.5	7.53
FeI	6330.85	4.73	-1.22	0.0	0.00	0.0	0.00	62.5	7.72
FeI	6335.34	2.20	-2.28	0.0	0.00	167.0	7.63	156.6	7.54
FeI	6392.54	2.28	-3.97	0.0	0.00	68.4	7.61	0.0	0.00
FeI	6411.66	3.65	-0.60	0.0	0.00	0.0	0.00	156.1	7.46
FeI	6436.41	4.19	-2.31	42.0	7.67	38.5	7.65	0.0	0.00
FeI	6518.37	2.83	-2.56	0.0	0.00	0.0	0.00	104.0	7.70
FeI	6533.94	4.56	-1.28	0.0	0.00	0.0	0.00	62.5	7.57
FeI	6591.31	4.59	-1.95	0.0	0.00	28.3	7.53	28.5	7.55
FeI	6633.76	4.56	-0.81	0.0	0.00	97.6	7.70	0.0	0.00
FeI	6667.43	2.45	-4.28	0.0	0.00	0.0	0.00	29.9	7.37
FeI	6667.72	4.58	-2.01	0.0	0.00	36.9	7.76	43.7	7.93
FeI	6699.14	4.59	-2.02	0.0	0.00	0.0	0.00	37.3	7.81
FeI	6703.58	2.76	-3.00	0.0	0.00	0.0	0.00	100.2	7.94
FeI	6704.48	4.22	-2.55	0.0	0.00	24.5	7.61	35.7	7.86
FeI	6725.36	4.10	-2.21	0.0	0.00	57.8	7.79	0.0	0.00
FeI	6726.67	4.61	-1.05	0.0	0.00	69.6	7.44	64.3	7.43
FeI	6733.15	4.64	-1.44	0.0	0.00	56.7	7.63	0.0	0.00
FeI	6750.16	2.42	-2.58	0.0	0.00	131.8	7.56	125.9	7.60
FeI	6753.47	4.56	-2.26	0.0	0.00	25.1	7.72	31.9	7.90
FeI	6756.55	4.29	-2.69	0.0	0.00	22.4	7.78	0.0	0.00
FeI	6786.86	4.19	-1.90	0.0	0.00	56.8	7.57	50.4	7.49
FeI	6793.26	4.07	-2.34	0.0	0.00	0.0	0.00	35.7	7.47
FeI	6796.12	4.14	-2.31	0.0	0.00	51.3	7.82	37.3	7.56
FeI	6806.86	2.73	-3.14	0.0	0.00	0.0	0.00	84.5	7.70
FeI	6810.27	4.61	-1.00	0.0	0.00	86.1	7.71	0.0	0.00
FeI	6820.37	4.64	-1.16	0.0	0.00	0.0	0.00	84.5	7.99
FeI	6843.66	4.55	-0.86	0.0	0.00	99.3	7.75	88.1	7.66
FeI	6851.64	1.61	-5.22	57.1	7.74	0.0	0.00	49.4	7.65
FeI	6855.72	4.61	-1.71	0.0	0.00	38.7	7.51	0.0	0.00
FeI	6858.16	4.61	-0.95	0.0	0.00	80.6	7.55	78.3	7.62

Table 3: Equivalent widths (cont...)

Element	Wavel.	E.P.	log gf	333		978		979	
FeI	6861.95	2.42	-3.78	0.0	0.00	71.3	7.60	68.5	7.61
FeI	6862.50	4.56	-1.43	0.0	0.00	60.8	7.60	55.5	7.56
FeI	6880.63	4.15	-2.23	0.0	0.00	49.5	7.71	28.6	7.31
FeI	6936.50	4.61	-2.14	0.0	0.00	29.2	7.75	15.7	7.38
FeI	6960.32	4.59	-1.88	0.0	0.00	0.0	0.00	49.1	7.90
FeI	6971.94	3.02	-3.35	0.0	0.00	64.6	7.76	0.0	0.00
FeI	7010.35	4.58	-1.84	37.4	7.54	33.0	7.50	0.0	0.00
FeI	7069.54	2.56	-4.20	0.0	0.00	39.8	7.63	34.3	7.49
FeI	7114.56	2.69	-3.87	0.0	0.00	43.6	7.51	0.0	0.00
FeI	7118.10	5.01	-1.50	0.0	0.00	38.1	7.73	28.4	7.56
FeII	5991.38	3.15	-3.55	52.0	7.49	52.0	7.55	0.0	0.00
FeII	6084.10	3.20	-3.80	0.0	0.00	31.9	7.36	34.2	7.65
FeII	6113.33	3.21	-4.12	0.0	0.00	35.6	7.79	17.4	7.45
FeII	6149.25	3.89	-2.72	0.0	0.00	0.0	0.00	37.1	7.43
FeII	6247.56	3.87	-2.32	0.0	0.00	76.4	7.69	60.1	7.64
FeII	6369.46	2.89	-4.21	0.0	0.00	34.4	7.50	0.0	0.00
FeII	6383.72	5.55	-2.09	20.6	7.77	0.0	0.00	0.0	0.00
FeII	6416.93	3.89	-2.70	0.0	0.00	0.0	0.00	53.2	7.86
FeII	6432.68	2.89	-3.58	0.0	0.00	0.0	0.00	54.1	7.61
FeII	6456.39	3.90	-2.10	0.0	0.00	84.7	7.68	0.0	0.00
CoI	5647.24	2.28	-1.56	0.0	0.00	68.8	5.00	74.0	5.25
CoI	6455.00	3.63	-0.25	57.5	4.91	60.5	5.04	36.2	4.60
NiI	5578.73	1.68	-2.57	0.0	0.00	118.4	6.53	0.0	0.00
NiI	5587.87	1.93	-2.39	0.0	0.00	98.3	6.17	0.0	0.00
NiI	5589.37	3.90	-1.15	49.9	6.13	0.0	0.00	0.0	0.00
NiI	5593.75	3.90	-0.78	0.0	0.00	64.3	6.13	0.0	0.00
NiI	5643.09	4.16	-1.25	0.0	0.00	39.3	6.37	0.0	0.00
NiI	5748.36	1.68	-3.25	0.0	0.00	94.5	6.61	67.7	6.15
NiI	5760.84	4.10	-0.81	0.0	0.00	54.7	6.18	0.0	0.00
NiI	5805.23	4.17	-0.60	0.0	0.00	65.4	6.26	0.0	0.00
NiI	5847.01	1.68	-3.44	0.0	0.00	74.3	6.37	0.0	0.00

Table 3: Equivalent widths (cont...)

Element	Wavel.	E.P.	log gf	333		978		979	
NiI	5996.74	4.23	-1.06	0.0	0.00	46.1	6.39	38.3	6.29
NiI	6053.69	4.23	-1.07	0.0	0.00	0.0	0.00	43.8	6.43
NiI	6086.29	4.26	-0.47	72.3	6.25	0.0	0.00	0.0	0.00
NiI	6108.13	1.68	-2.47	130.0	6.25	124.6	6.40	122.2	6.56
NiI	6111.08	4.09	-0.83	72.9	6.42	60.6	6.28	57.4	6.33
NiI	6128.98	1.68	-3.39	74.9	6.15	82.4	6.43	0.0	0.00
NiI	6130.14	4.26	-0.98	0.0	0.00	49.6	6.40	0.0	0.00
NiI	6322.17	4.15	-1.21	0.0	0.00	0.0	0.00	38.6	6.34
NiI	6327.60	1.68	-3.08	0.0	0.00	0.0	0.00	95.4	6.53
NiI	6482.81	1.93	-2.78	0.0	0.00	0.0	0.00	87.2	6.35
NiI	6586.32	1.95	-2.78	0.0	0.00	103.5	6.53	100.0	6.65
NiI	6598.61	4.23	-0.93	0.0	0.00	53.3	6.37	0.0	0.00
NiI	6767.78	1.83	-2.06	0.0	0.00	148.0	6.45	138.9	6.45
NiI	6772.32	3.66	-0.96	0.0	0.00	0.0	0.00	90.0	6.63
Y II	5544.62	1.74	-1.09	0.0	0.00	23.2	2.33	30.5	2.64
BaII	6496.91	0.60	-0.38	0.0	0.00	0.0	0.00	120.6	2.17

Table 4: Average abundances. The adopted solar abundances are in the second column (they were obtained from an inverted solar analysis, using Kurucz model atmospheres and equivalent widths from the literature for the same set of lines used for the stars). For each star we give the number of lines, the average abundance (in the scale $\log n(A)$, where $\log n(H) = 12$), the r.m.s. of individual lines around this average value, and the overabundance with respect to Fe, save for Fe for which we give the $[\text{Fe}/\text{H}]$ value. The last column give the average overabundances ($[\text{Fe}/\text{H}]$ values for Fe) for NGC6819; the error bars were obtained as explained in the text

El.	Sun	333				978				979				$< [\text{A}/\text{Fe}] >$
Fe I	7.52	49	7.62	0.16	+0.10	90	7.60	0.12	+0.08	90	7.61	0.20	+0.09	+0.09 ± 0.03
Fe II	7.52	2	7.63	0.14		6	7.60	0.15		6	7.61	0.16		
Na I	6.23	2	6.68	0.11	+0.35	1	6.96		+0.65	3	6.72	0.37	+0.40	+0.47 ± 0.07
Mg I	7.48	1	7.50		-0.08	1	7.65		+0.09	3	7.20	0.10	-0.37	-0.12 ± 0.07
Al I	6.30	1	6.35		-0.05	1	6.44		+0.06	2	6.17	0.32	-0.22	-0.07 ± 0.07
Si I	7.55	7	7.65	0.10	+0.03	8	7.82	0.14	+0.19	8	7.96	0.16	+0.32	+0.18 ± 0.04
Ca I	6.18	4	6.34	0.25	+0.06	2	6.30	0.55	+0.04	3	6.04	0.22	-0.23	-0.04 ± 0.06
Sc I	3.10		1	3.21		+0.03		..			+0.02 ± 0.13
Sc II	3.10	3	3.13	0.13	-0.07	5	3.30	0.08	+0.12	5	3.28	0.12	+0.06	+0.04 ± 0.04
Ti I	4.94	3	5.06	0.09	+0.02	7	5.22	0.16	+0.20	4	4.78	0.14	-0.25	-0.01 ± 0.04
V I	3.93	5	4.12	0.10	+0.09	2	3.98	0.12	-0.03	3	3.70	0.24	-0.32	-0.09 ± 0.07
Cr I	5.63	3	5.68	0.27	-0.05	3	5.60	0.14	-0.11	5	5.59	0.25	-0.13	-0.10 ± 0.05
Mn I	5.47	3	5.54	0.11	-0.03	1	5.66		+0.11	1	5.70		+0.14	+0.07 ± 0.08
Co I	4.94	1	4.91		-0.13	2	5.02	0.03	0.00	2	4.93	0.45	-0.10	-0.08 ± 0.05
Ni I	6.25	5	6.24	0.11	-0.11	16	6.37	0.14	+0.04	11	6.43	0.15	+0.09	+0.01 ± 0.02
Y II	2.24		1	2.34		+0.02	1	2.64		+0.31	+0.16 ± 0.10
Ba II	2.34		1	2.16		-0.27	-0.27 ± 0.15

Table 5: Sensitivity of abundances to atmospheric parameters

	ΔT_{eff}	$\Delta \log g$	$\Delta [A/H]$	Δv_t	total
	+100 K	+0.3 dex	+0.1 dex	+0.2 km ⁻¹	
[Fe/H]I	+0.059	+0.016	+0.010	-0.057	0.048
[Fe/H]II	-0.082	+0.159	+0.037	-0.061	0.128
[Na/Fe]	+0.029	-0.066	-0.010	-0.018	0.129
[Mg/Fe]	-0.015	-0.016	-0.003	+0.029	0.121
[Al/Fe]	+0.013	-0.032	-0.013	+0.016	0.122
[Si/Fe]	-0.078	+0.036	+0.010	+0.016	0.072
[Ca/Fe]	+0.082	-0.072	-0.016	-0.046	0.113
[Sc/Fe]	+0.070	-0.037	-0.009	-0.043	0.077
[Ti/Fe]	+0.076	-0.024	-0.018	-0.028	0.071
[V/Fe]	+0.107	-0.016	-0.022	-0.049	0.114
[Cr/Fe]	+0.050	-0.022	-0.016	-0.004	0.079
[Mn/Fe]	+0.035	-0.072	-0.003	-0.080	0.133
[Co/Fe]	+0.001	+0.031	+0.003	-0.008	0.087
[Ni/Fe]	-0.013	+0.034	+0.006	-0.040	0.040
[Y/Fe]	+0.067	-0.027	+0.001	+0.043	0.130